

Seismicity of the Askja and Bárðarbunga volcanic systems of Iceland, 2009–2015

Tim Greenfield*, Robert S. White, Tom Winder, Thorbjörg Ágústsdóttir

Bullard Laboratories, University of Cambridge, Madingley Road, Cambridge CB3 0EZ, United Kingdom

ARTICLE INFO

Article history:

Received 23 December 2017

Received in revised form 18 June 2018

Accepted 23 August 2018

Available online 28 August 2018

Keywords:

Seismicity

b-Value

Earthquake magnitude

Iceland

Askja

Triggering

Bárðarbunga

ABSTRACT

A large seismic network deployed in the Icelandic highlands recorded >100,000 earthquakes from 2009 to 2015. We develop a local magnitude scale, appropriate for use in central Iceland, which is similar to the scale used by the Iceland Meteorological Office. Using this large catalogue of earthquakes, we analyze the spatial and temporal changes in seismicity rates and b-values. In microearthquakes recorded from the usually ductile lower crust we find that b-values are high, reflecting the presence of high thermal gradients and low stresses driving seismicity associated with the movement of melt. In contrast, b-values in the upper crust are variable. Low b-values, indicative of a high stress environment, are observed during seismic swarms such as those around Mt. Herðubreið and around Bárðarbunga caldera. A persistently seismically active area around a geothermal area within Askja caldera has a b-value around 1 but has a strong annual cycle of seismicity. We attribute the annual cycle to varying load from the snow cover modulating the seismicity. Seismicity driven by the intrusion of a large dyke has a b-value well above 1, driven by the high pore fluid pressures and thermal gradients around the dyke.

© 2018 The Authors. Published by Elsevier B.V. This is an open access article under the CC BY license (<http://creativecommons.org/licenses/by/4.0/>).

1. Introduction

Seismic networks around active volcanoes often record large numbers of earthquakes during both restless and quiescent phases. However, data is often only analyzed in detail and published during restless phases when a crisis seems imminent. In this study, a long duration (2009–2015) dense seismic network is used to detect and locate seismicity in the central part of the northern volcanic rift zone in Iceland, straddling the Askja and Bárðarbunga central volcanoes and their associated rift segments (Fig. 1). By good fortune, a dyke intrusion and subsequent eruption from the volcano Bárðarbunga was captured by the network, while the Askja segment was both magmatically and tectonically active. This allows us to examine and compare both quiescent and restless phases from the same system. A new local magnitude scale for micro-earthquakes is developed, appropriate for use in central Iceland. The frequency-magnitude relationships of the detected earthquakes are analyzed both spatially and temporally, revealing the different processes causing seismicity along these rift systems.

Askja is a large central volcano in the Northern Volcanic Zone (see inset, Fig. 1 for location), north of the Vatnajökull ice sheet. The edifice is composed primarily of hyaloclastite and basaltic lava flows. Evidence of at least three caldera forming eruptions is present, with the youngest located in the south-east corner and filled by the lake Öskjuvatn. This

lake was formed during a rifting episode in 1875 which culminated in a sub-Plinian rhyolitic eruption (Carey et al., 2010). Numerous small basaltic fissure eruptions occurred in the first half of the 20th century around the edge of lake Öskjuvatn. The most recent eruption was in 1961 when a small fissure erupted for 5 weeks in the north-east corner of the largest caldera (Thorarinnsson, 1962). Several geothermal areas associated with the ring fault system occur around the lake Öskjuvatn. Steam vents and regions with elevated surface temperatures are found on the western, southern and eastern shores of the lake. Within the lake, bubbles are often seen rising from a portion of the lake that is rarely frozen over during the winter, suggesting heat input from beneath.

Askja has been studied geodetically for the last 50 years, first using a levelling line and more recently using InSAR and GPS. All studies report an exponentially decaying subsidence of Askja since at least 1983, which can be modelled as depressurization of a shallow Mogi source (de Zeeuw-Van Dalssen et al., 2005; Sturkell et al., 2006; de Zeeuw-Van Dalssen et al., 2013), in combination with plate spreading processes (Pedersen et al., 2009). Local earthquake tomography reveals the presence of a large low-velocity region at 5 km depth below sea level (bsl) centred beneath Askja. This is interpreted as the primary melt storage region (Greenfield et al., 2016). At a depth of 2 km bsl, similar to the depth and location of the Mogi source inferred by modelling the subsidence, a seismically attenuating region is present beneath the largest of three Askja calderas.

In contrast, less is known about Bárðarbunga. This is mainly due to the difficulty in instrumenting a volcano located beneath an ice sheet.

* Corresponding author at: Now at School of Ocean and Earth Sciences, University of Southampton, European Way, Southampton SO14 3ZH, United Kingdom.
E-mail address: t.s.greenfield@soton.ac.uk (T. Greenfield).

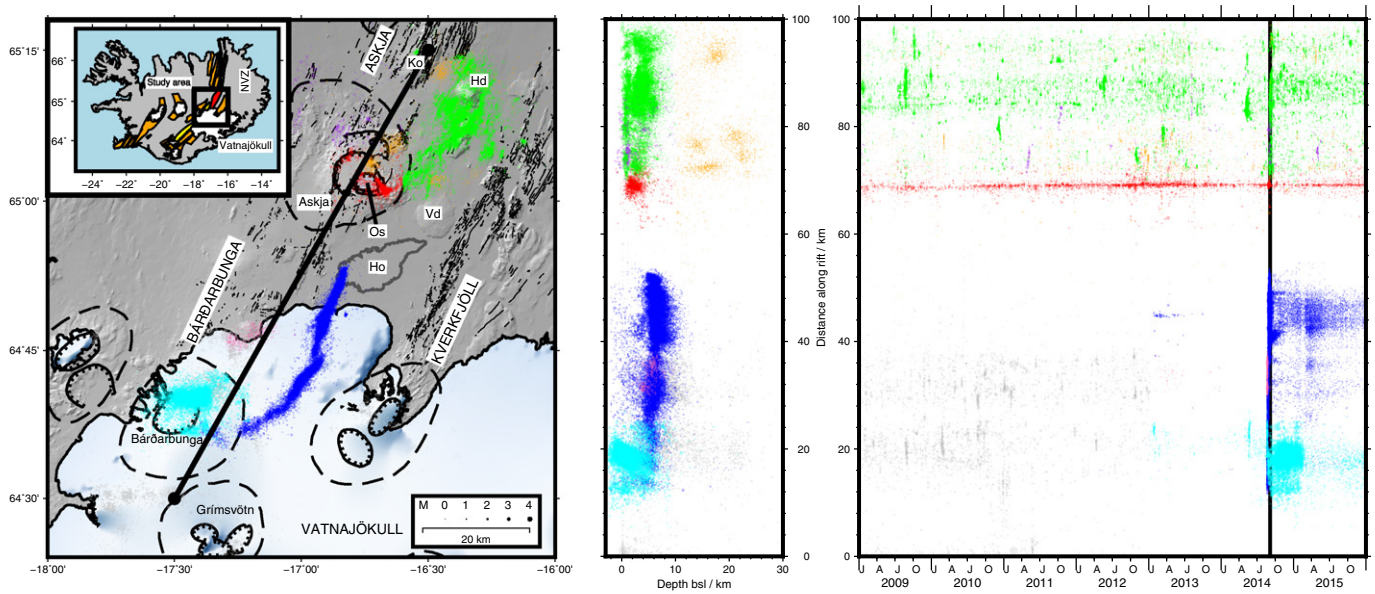


Fig. 1. Location map and seismicity of central Iceland, January 2009–December 2015. Left panel delineates central volcanoes (dashed lines) and calderas (ticked lines). The Askja, Bárðarbunga and Kverkfjöll fissure swarms are labelled and orientated along the rift. The location of features named in the text are labelled as: Askja volcano (Askja), Vaðalda (Vd), Kollotadyngja (Ko), Öskjuvatn (Os), Herðubreið (Hd), Vatnajökull icesheet (Vatnajökull), Bárðarbunga volcano (Bárðarbunga) and Grímsvötn Volcano (Grímsvötn). The final extent of the lava flow from the Bárðarbunga-Holuhraun eruption is outlined and labelled Ho. Inset map shows the location of the study area in Iceland compared to the volcanic systems (orange areas) and glaciers (white). The Vatnajökull icesheet is labelled. The Askja and Bárðarbunga rift segments are coloured red and yellow respectively. The location of the Northern Volcanic Zone is labelled as NVZ. Earthquakes are scaled by magnitude according to the scale shown in the lower-right panel. In all panels red coloured earthquakes are from the Askja catalogue, green earthquakes the Herðubreið catalogue, dark blue earthquakes the Bárðarbunga dyke and light blue earthquakes the Bárðarbunga caldera. Orange coloured earthquakes are those located around Askja deeper than 10 km bsf. Earthquakes coloured purple and pink are the West Askja and Kistufell clusters respectively. The location of a cross section from south to north along the rift is delineated by the black line. Middle panel shows the depth distribution of the seismicity projected on to this section. Right panel shows time series of earthquakes against distance along the rift using the same colour code.

Ice penetrating radar has revealed the existence of a large caldera beneath the ice with an area of 80 km² (Larsen and Gudmundsson, 2015). Around the edge of the caldera, a few ice cauldrons suggest that there are active geothermal systems present. As one of the more active volcanoes in Iceland, Bárðarbunga is known to have erupted at least 26 times in the last 1100 years (Larsen and Gudmundsson, 2015). These include some of the most voluminous eruptions documented in Iceland. The last eruption before the dyke intrusion in 2014 was the Gjalp eruption beneath Vatnajökull during 1996. This was triggered by a dyke injection from Bárðarbunga (Einarsson et al., 1997) but has a geochemical fingerprint from Grímsvötn, suggesting that the dyke may have intersected or triggered the release of a pre-existing melt pocket (Sigmarsson et al., 2000; Sigmarsson and Halldorsson, 2015).

The dyke intrusion in 2014 and subsequent 6 months long fissure eruption caused major changes to the rate and location of seismicity in the region covered by this study. On 16th August 2014 a large seismic swarm indicated the start of a dyke intrusion which ended two weeks later in a major eruption (Ágústsdóttir et al., 2016). A 48 km long dyke was intruded to the NE, with up to 6 m of opening (Sigmondsson et al., 2015). The Bárðarbunga caldera subsided 65 m during the eruption as a result of melt leaving an upper crustal storage region (Gudmundsson et al., 2016).

2. Methods

2.1. Seismic network

A network of 3-component seismometers has been deployed by the University of Cambridge in the Icelandic highlands since 2008. Initially this was focused around Askja, with a network of 16 instruments. The network increased in both the number of instruments and the area covered so that by August 2014 both Askja and Bárðarbunga were covered by over 70 seismometers. The earthquake

catalogue reported here for Askja is continuous back to January 2009, while the Bárðarbunga catalogue is continuous back to January 2013. In the data reported here, both catalogues end on 31 December 2015, although the network is still operational at the time of writing (2018).

The seismic network primarily uses Güralp 6TDs, three-component broadband seismometers with a 30 s corner frequency. A smaller number of Güralp 3ESPCDs (60 s corner frequency), and Güralp 3Ts (120 s corner frequency) with Nanometrix Taurus digitizers were also deployed. Güralp 6TDs were mostly buried directly in the sand/ash whereas the instruments with lower corner frequencies were deployed in small vaults built directly on bedrock. During the winter months, the buried instruments became frozen into the ground, which provided excellent coupling. Data was recorded internally at 100 samples per second. With 16 GB flash storage, this allowed 10–11 months of continuous data to be saved on the 6TDs. The quieter ESPCDs and 3Ts were capable of saving a full year of data. Data were downloaded in the field twice a year: at the start of the field season in early July and subsequently in early September. All instruments were powered using solar panels and large batteries. In general, during the darker winter months, instruments relied on battery power alone and some sites had to contain sufficient battery capacity (typically 500 Ahr) to last from November to May while solar panels were covered in snow. The snow also masked the GPS signal at some sites and care was taken to ensure GPS antennae were higher than the snow all year.

Despite the difficulties of operating in the Icelandic highlands, which are typically 1000 m above sea level and close to the Arctic Circle, data recovery was in general better than 80% and improved to nearly 100% as the project continued and our power management improved. The raw data from the seismometers was converted into standard MiniSEED format and quality controlled to remove periods when the data were unreliable. This was mainly due to problems with the GPS timing signal, either because of instrument failure or from blocking of the signal by ice on the GPS antenna.

2.2. Earthquake catalogue

Earthquakes are detected and located automatically using the Coalescence Microseismic Mapping (CMM) software (Drew et al., 2013). This technique uses the ratio between a short-term-average (STA) and a long-term-average (LTA) of the recorded data across a seismic network to generate a characteristic function on each station. When this ratio is higher than a predefined threshold a Gaussian function is fitted, the width of which is proportional to the uncertainty in the P-wave or S-wave arrival. This function is continually migrated into a network of nodes in the subsurface and when the energy detected at multiple stations coalesces at a node, an earthquake is defined as having occurred close to that node. The technique avoids potential bias due to mispicked discrete arrival times on noisy time-series because mispicks will not contribute to the coalesced data at the correct location and origin time. The use of both P- and S-wave energy simultaneously results in accurate and robust earthquake locations.

CMM uses a predefined grid of travel times to every station in the network to locate the events. Travel time grids are calculated for each station using separate 1D velocity models for the Bárðarbunga and Askja regions (see Supplementary Information Table 1 for details). In the Bárðarbunga region, the velocity model is the same as that used by Ágústsdóttir et al. (2016). The velocity model used in the Askja area is from Greenfield et al. (2016). Events which occur outside the travel time grid (such as regional or teleseismic earthquakes) are typically mis-located to the edge of the grid. These artefacts are removed by only accepting events which are located >5 km from the grid edges. Results are also filtered using the output signal-to-noise (SNR) ratio and reported errors. Typically, events with a SNR ratio of the coalesced signal above 2 are likely to be real using the parameters appropriate for central Iceland. We relocate the detected seismicity using NonLinLoc (Lomax et al., 2000). Phase arrivals which do not fit the calculated hypocenter are internally downweighted in NonLinLoc, leading to an improvement in the reported depths of the earthquake catalogue and absolute error estimations.

2.3. Magnitudes

The seismic waveforms recorded at each station are cut from the continuous data to generate waveforms for each earthquake. The response of the recording instrument is removed from these waveforms after de-meaning and tapering the data. The response of a standard Wood-Anderson seismograph is convolved with the waveforms using the corrected gain of 2080 (Urhammer, 1982). The maximum zero-to-peak amplitude is then picked automatically on each horizontal component. We do this across all stations in the network and require the maximum amplitude to be greater than twice the standard deviation of a 10 s portion of the data recorded before the P-wave arrival time. This ensures that only data which record good arrivals from each earthquake are used to calculate the magnitude.

For the low magnitude microseismicity recorded around Askja and Bárðarbunga a local magnitude scale is used. Such a scale was first derived by Richter (1935) to be used in southern California. The magnitude scale is fixed to a reference earthquake size and distance which was initially that a magnitude 3 earthquake should generate 1 mm of displacement on a standard Wood-Anderson seismograph at 100 km distance. A parameter $\log(A_0)$ in the equation below corrects observations to this standard scale. It is analogous to the effect of attenuation in the region.

$$M_i = \log(A_{ijk}) - \log(A_0) + C_{jk}$$

where M_i is the magnitude of earthquake i , A_{ijk} is the amplitude recorded at station j , and component (north-south or east-west) k , in mm and C_{jk} is the correction term for a specific station-component combination.

Hutton and Boore (1987) showed that the choice of reference event at 100 km distance was not appropriate because the attenuation curve derived by Richter (1935) did not account for the attenuation structure

at shorter epicentral distances. Instead, a new reference event was proposed: a magnitude 3 earthquake recorded at 17 km distance should produce a displacement of 10 mm. This was consistent with the originally derived $\log(A_0)$ parameter. Using 17 km as the reference distance the $\log(A_0)$ parameter can be formulated as:

$$-\log(A_0) = n \log\left(\frac{r_{ij}}{17}\right) - K(r_{ij} - 17) + 2$$

where n and K are constants to be calibrated and r_{ij} is the hypocentral distance.

The magnitudes M_i , station corrections C_{jk} , and constants n and K are calculated by combining all amplitude observations into a matrix and inverting directly for the parameters using a least-squares approach. This follows the method used by Keir et al. (2006) and Illsley-Kemp et al. (2017).

Inversions were completed for the Askja and Bárðarbunga catalogues separately, as well as for a single combined catalogue, to investigate how much the attenuation structure varies across this area of Iceland. The calculated attenuation curves ($-\log(A_0)$) are shown in Fig. 2 and summarized in the equations below. All curves are valid to hypocentral distances of 150 km.

$$\text{Askja : } -\log(A_0) = 1.4406 \log(r_{ij}/17) + 0.0030(r_{ij} - 17) + 2$$

$$\text{Bárðarbunga : } -\log(A_0) = 1.2534 \log(r_{ij}/17) - 0.0032(r_{ij} - 17) + 2$$

$$\text{Combined : } -\log(A_0) = 1.1999 \log(r_{ij}/17) - 0.0016(r_{ij} - 17) + 2$$

Magnitudes calculated in this study are similar to local magnitudes recorded by IMO (Fig. 3). At larger magnitudes ($M > 3.5$) our local magnitude scale underestimates the moment magnitude. This is a result of the application of the Wood-Anderson seismograph response. This response is sensitive to frequencies of 1 Hz and acts as a high-pass filter, removing the highest amplitude waves. The reported magnitudes (Supplementary Dataset 1) are calculated using the appropriate equation for the region. Earthquakes south of 64.9° are calculated using the Bárðarbunga equation and those north of 64.9° are calculated using the Askja equation.

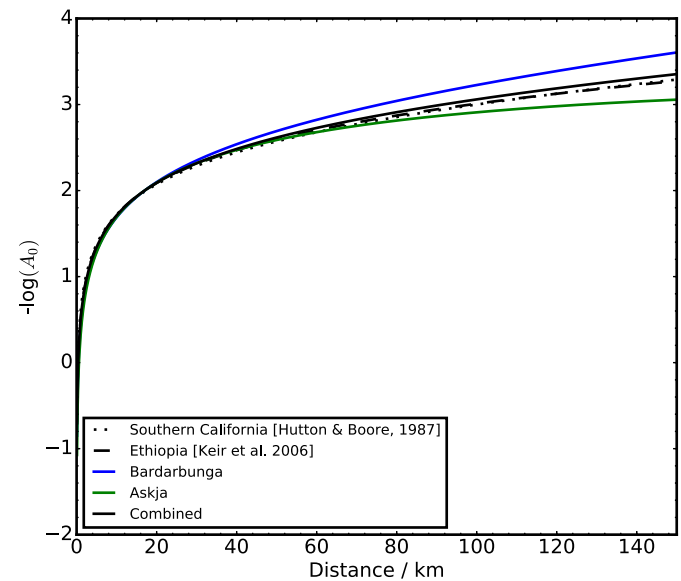


Fig. 2. $\log(A_0)$ curves inverted using the Askja catalogue (green line), the Bárðarbunga catalogue (blue line) and both catalogues together (black line) For comparison the curves from Southern California (dotted black line) and Ethiopia (dashed black line) are also plotted.

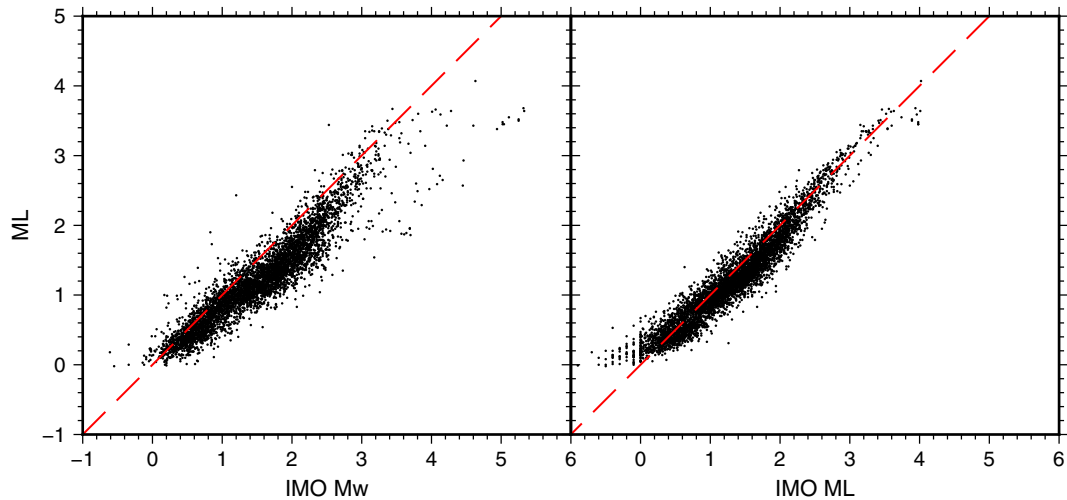


Fig. 3. Comparison for the same earthquakes of the local magnitude scale reported in this paper with that developed by the Icelandic Meteorological Office (IMO). The IMO report both a local magnitude ML and a moment magnitude Mw for each event.

2.4. *b*-values

Typical earthquake catalogues obey the Gutenberg-Richter distribution at larger magnitudes:

$$\log_{10}N = a - bM$$

where N is the number of earthquakes greater than magnitude M , a and b are constants and express the overall rate of seismicity and the relative weighting of large earthquakes to small ones respectively. Globally b is found to be close to 1 (El-Isa and Eaton, 2014), implying for example that there are ten times more magnitude 2 events than magnitude 3 events.

Regional and temporal variations in the b -value reflect changes in the power law scaling parameter. Experimentally it has been shown that the b -value is inversely proportional to the stress of the system (Scholz, 1968) and proportional to the thermal gradient in an area (Latham and Warren, 1970). This reflects the fault density of a region. Where there are many faults with different orientations, failure occurs on many small planes or is prevented from propagating by the crossing of two faults. This causes the b -value to increase. Around volcanic regions, changes in the effective stress and thermal gradient are expected causing significant changes in the value of b .

Seismic networks have a finite detection threshold which can be expressed as a magnitude of completeness (M_c), above which the network has detected every event. In seismically quiet regions with a high density of stations the value of M_c is small and vice-versa. This causes the number of earthquakes detected at magnitudes lower than M_c to be fewer than that predicted by the Gutenberg-Richter relationship. When fitting an observed distribution to find the value of b it is therefore important only to include earthquakes with magnitudes above M_c .

M_c is usually picked as the magnitude bin containing the highest number of earthquakes (e.g. Fig. 4). This is a proxy for the point of maximum curvature in the Gutenberg-Richter distribution. However, temporal and spatial changes in M_c due to alterations and additions to the seismic network and changeable noise conditions may result in incorrect values of M_c using this criterion. The value calculated from the bin containing the maximum number of earthquakes is typically lower than the actual value of M_c because rather than a hard cut-off in the detected number of events there is a magnitude range over which events may or may not be detected, depending on the condition of the network at that exact time.

An alternative technique is the b -value stability criterion (Cao and Gao, 2002; Roberts et al., 2015) in which a trial value of M_c is varied

from low to high magnitudes with a step length, Δm (Fig. 4). A b -value is calculated for each possible value of M_c . When the b -value is the same (within error) as a forward rolling mean with a window of length $5\Delta m$ the value of M_c is recorded, along with the accompanying value of b and its error.

The value of b is determined analytically using the equation of Aki (1965), modified to take into account the uneven distribution of events in the binned distribution compared to a continuous function:

$$b = \left(\frac{1}{\ln(10)} \right) \left(\frac{1}{\mu - (M_{min} - \Delta M/2)} \right)$$

$$\sigma = 2.3b^2 \sqrt{\frac{1}{T(T-1)} \sum_{i=1}^T (M_i - \mu)^2}$$

where μ is the mean magnitude, M_{min} is the minimum magnitude, T is the total number of earthquakes, M_i is the magnitude of earthquake i , σ is the error in the value of b and ΔM is the bin width used (Shi and Bolt, 1982). Note that the error in b is proportional to the value of b .

Due to significant changes in the seismic network between 2009 and 2015 as well as marked differences in noise levels between seasons and across the region, this study uses the b -value stability criterion to determine M_c and subsequently to calculate b (Fig. 4).

2.4.1. *b*-value temporal variations

The difficulty in estimating reliably the value of b has limited the interpretation of temporal changes in the b -value. We apply a probabilistic technique based on that proposed by Roberts et al. (2016) to analyze the temporal variation in the b -value around Askja and Bárðarbunga. The technique avoids biases generated because of the choice of window length by using randomly sized windows. The technique proceeds as follows:

1. The earthquake catalogue is split into many randomly different length windows of length between 50 and 2000 earthquakes.
2. The windowing procedure is repeated 200 times to generate 200 differently windowed earthquake catalogues. Importantly, to avoid biases in the window length at the start and end of the earthquake catalogue, the first 100 catalogues are generated with the windows starting at the end and the final 100 catalogues are generated with the windowing starting at the beginning.
3. The b -value and associated error are calculated for each window and assigned a time stamp calculated from the mean origin time of the

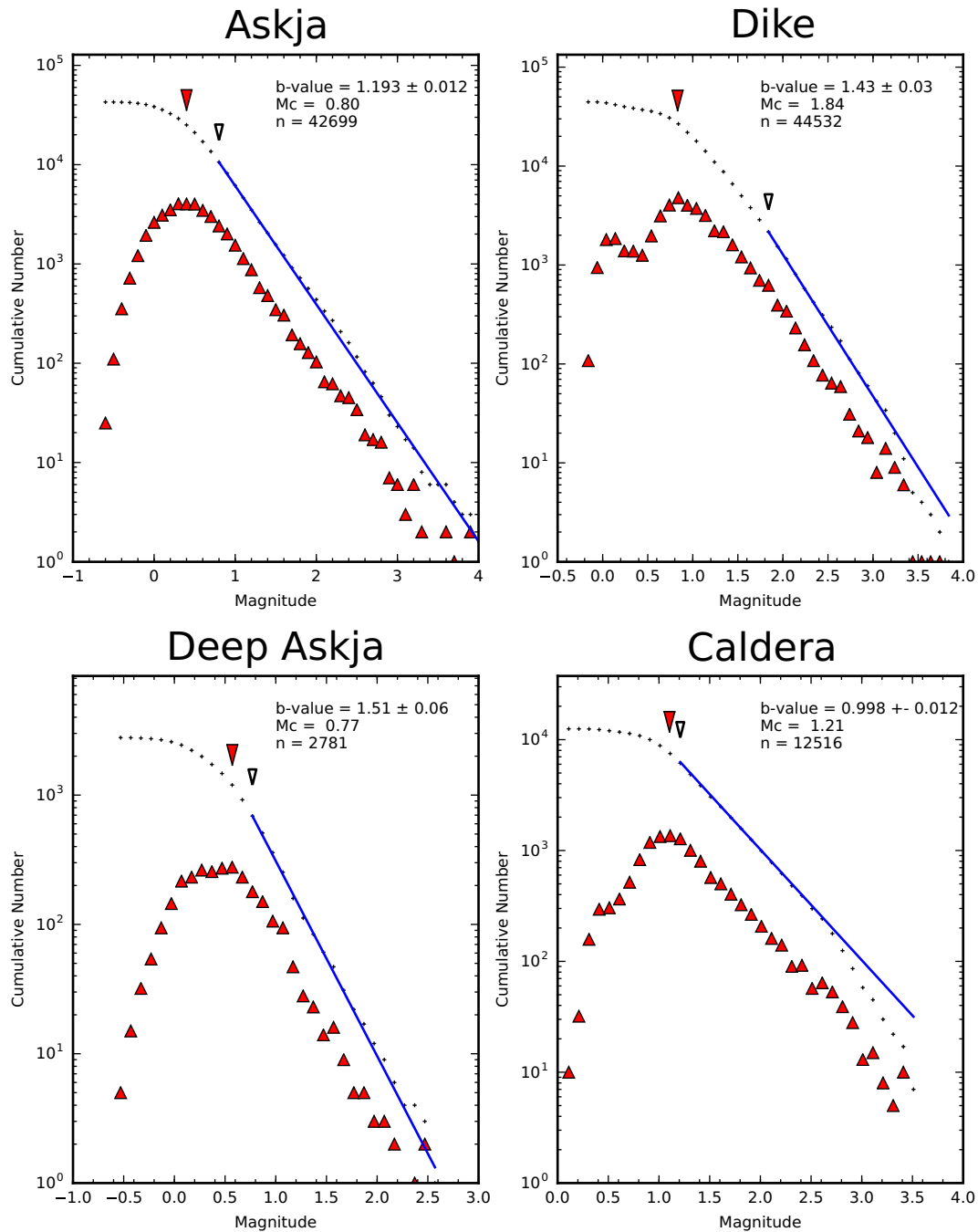


Fig. 4. Example earthquake magnitude-frequency distributions for the Askja volcano catalogue (upper left), Bárðarbunga dyke (upper right), Bárðarbunga caldera (lower right) and earthquakes located deeper than 10 km bsl around Askja (lower left). The number of earthquakes in each magnitude bin is indicated by the red triangles and the cumulative number by the small black crosses. The magnitude of completeness (M_c) calculated using the maximum curvature method is indicated by the large red inverted triangle. The preferred M_c , calculated using the b-value stability criterion is indicated by the white inverted triangle. The gradient fitted to the data using the maximum likelihood estimation is delineated by the blue line. The final b-value, M_c and number of earthquakes (n) is quoted in the top right of each panel.

earthquakes in the window. The b-value is then converted to a probability density function (PDF) using a normal distribution.

4. The final PDF is calculated by summing a fixed number of individual PDFs. After normalizing, such that the sum over all b is equal to 1, we assign a time stamp to the stack using both the mean origin time of the stacked windows and the mean event number. We follow the results of [Roberts et al. \(2016\)](#) and use 50 as the number of windows to stack.

We image the PDF by making contour plots in probability-time space.

3. Results and discussion

3.1. Earthquake catalogue

The total number of earthquakes detected and located around Bárðarbunga and Askja between January 2009 and December 2015 are ~100,000. Of this 58,255 are located around Bárðarbunga and are associated mainly with the 48 km long dyke intrusion and subsequent eruption in August 2014. The seismicity associated with the intrusion and subsequent eruption at Holuhraun has been studied previously ([Green et al., 2015](#);

Sigmundsson et al., 2015; Ágústsdóttir et al., 2016; Woods et al., 2018) and is not discussed in detail here.

In the Askja region, background rates of seismicity are generally high, with an average rate of 12 earthquakes per day prior to the 2014 Bárðarbunga dyke intrusion. Northeast of Askja volcano, intense seismic swarms occur once or twice per year and increase the average rate to 18 earthquakes per day overall for the same period. These seismic swarms between Askja and Herðubreið were studied by Green et al. (2014), who concluded that the observed left-lateral strike-slip faulting could be explained by northeast-southwest orientated bookshelf faults accommodating differential extension between the Askja and Kverkfjöll rift segments (see Fig. 1 for location). More recent work shows that these northeast-striking left-lateral faults form part of a conjugate set of strike-slip faults which between them accommodate the extension caused by plate spreading in a direction of 106° across this rift (Árnadóttir et al., 2009; DeMets et al., 2010). Fault plane solutions show that the north-south striking set comprises right-lateral faults (light green in Fig. 5), while the northeast-southwest set are all left-lateral (dark green in Fig. 5).

This area of the Askja rift system experienced a surge of seismicity during and following the 2014 Bárðarbunga-Holuhraun dyke intrusion. The step change in both the frequency of earthquakes and in moment release is the biggest observed in this part of the rift. It can be explained by the increase in Coulomb stress on faults in the Askja region caused by the opening associated with the dyke intrusion to the south. Using the receiver fault geometry defined by the fault plane solutions, we find that there is an increase in Coulomb stress on both the right-lateral and left-lateral strike slip faults, which moves both sets of faults closer to failure. Calculated Coulomb stresses are <1 bar (0.1 MPa) at the depth where the earthquakes are nucleated (Fig. 6). Given that the shear strength of intact basalt is ~50 MPa, the triggered faults must already be close to failure and occur in areas which are previously fractured.

The remaining seismicity around Askja can be split into three regions (Fig. 1): around Askja caldera, to the northwest of Askja and below the brittle-ductile transition. Seismicity located below the brittle-ductile boundary (c. 7 km below sea level) occurs in swarms but has an overall average rate of one earthquake per day. Such seismicity has been the focus of a number of studies (Soosalu et al., 2010; Key et al., 2011a; Key et al., 2011b; Greenfield and White, 2015) which all concluded that this seismicity is due to the active intrusion of melt into the lower to mid-crust.

The seismicity observed to the northwest of Askja forms a diffuse cluster. This region was only active during two swarms in 2009 and 2011, before many seismic stations were installed in this region. Because there is only a low station density in this area, the depth control on these earthquakes is poorer than for the other regions around Askja, and most fault plane solutions for this cluster are therefore unreliable. The few solutions that do exist suggest that the earthquakes have a normal mechanism, different to the strike-slip mechanisms found around Herðubreið. Normal faulting earthquakes are relatively rare in Iceland because regions with transform tectonics (i.e., Tjörnes Fracture Zone and South Iceland Seismic Zone) are more seismogenic and in general the extensional component of the plate spreading is accommodated by dyking during rifting episodes and strike-slip faulting (Karson, 2017).

A large number of earthquakes are located within the Askja caldera itself, divided into three clusters (Fig. 7): in the northeast corner of the main caldera, to the north of Öskjuvatn, and the main cluster to the southeast of Öskjuvatn. The depth distribution of this seismicity shows a peak at 2.8 km bsl (right hand panel, Fig. 7). In a similar setting, shallow seismicity is observed around Krafla where an active hydrothermal system is currently being exploited to generate geothermal energy (Schuler et al., 2016). The active geothermal area in Askja is located around Öskjuvatn, but is concentrated on the eastern side of the lake, in a similar location to the main cluster of seismicity and region with

low Vp/Vs ratios (Greenfield et al., 2016). The high pore fluid pressures, temperature gradients and active fluid flow in geothermal systems likely causes the seismicity.

The other clusters in the caldera are not associated with currently active geothermal systems. The cluster to the north of Öskjuvatn is associated with the eruption vents from Askja's most recent eruption in October 1961. Cooling of a shallow intrusive complex associated with this eruption could cause the observed seismicity. In the north-west corner of the main caldera, the third cluster is located beneath the caldera wall and some undated scoria cones. Two possible causes of this cluster are a cooling shallow intrusive body associated with the scoria cones or small amounts of motion along the caldera wall associated with the ongoing subsidence of Askja.

3.1.1. Seasonal variability

Initial observations of the earthquake time series suggest a seasonal variability in the number of detected earthquakes around the Askja caldera (Fig. 8). To analyze this, we first exclude data from after January 2014 because the surge in seismicity triggered by the dyke-induced stress change that strongly overprints and obscures the seasonal trend. An additional cause of seasonal variability in the number of detected events is the number of available stations (Supplementary Fig. 2). To account for the changing network geometry, we calculate the change in the magnitude of completeness for different periods of the year and throughout the duration of the experiment. During the winter the magnitude of completeness is typically 0.1 units higher than during the summer when all stations are recording. Therefore we then only include earthquakes which have a magnitude higher than the maximum observed magnitude of completeness (ML 0.2).

After filtering the earthquake catalogue we bin earthquake counts into equal length time windows and remove any linear trend. We use the multitaper FFT library from Prieto et al. (2009) to calculate the power spectral density (Supplementary Fig. 1). To test for periodic components in the spectrum we use the F-statistic output by the library (bottom panel, Fig. 8). A clear peak, well above the 95% likelihood and close to 99% likelihood is observed at periods close to 1 year. We confirm the strong statistical likelihood that such observations are not the result of random processes by performing a Schuster Test (Schuster, 1897; Ader and Avouac, 2013). We transform the origin times of the earthquakes into phase assuming a period of one year. The probability of such a distribution being random is then given by:

$$p = \exp\left(-\frac{L^2}{N}\right)$$

where L is then total length of the unit phasors and N is the total number of earthquakes. p values of <0.05 indicate that such a distribution is not likely to be random. The Askja seismicity has a p of <10⁻⁴⁰ indicating that the distribution is extremely unlikely to be random.

Seasonal changes in the observed ground deformation of Iceland have recently been studied using the Global Positioning System (GPS) (Drouin et al., 2017). In their study, observed GPS data and snow loading are fitted using the equation:

$$D(t) = a + bt + d \sin 2\pi t + e \cos 2\pi t + f \sin 4\pi t + g \cos 4\pi t$$

where D is the observed deformation at time t , a and b are constants which describe the linear trend and d , e , f and g are constants which describe the annual and semi-annual changes. We fit the observed earthquake time series to the same equation (upper and middle panel, Fig. 7) (Supplementary Table 1). Results suggest that a minimum in the number of earthquakes occurs around Julian day 100 and a maximum occurs around day 220.

The dominant cause of ground deformation in Iceland is because of snow accumulation (Drouin et al., 2017). The ground deformation is observed to be asymmetric through the year due to the slow build-up of

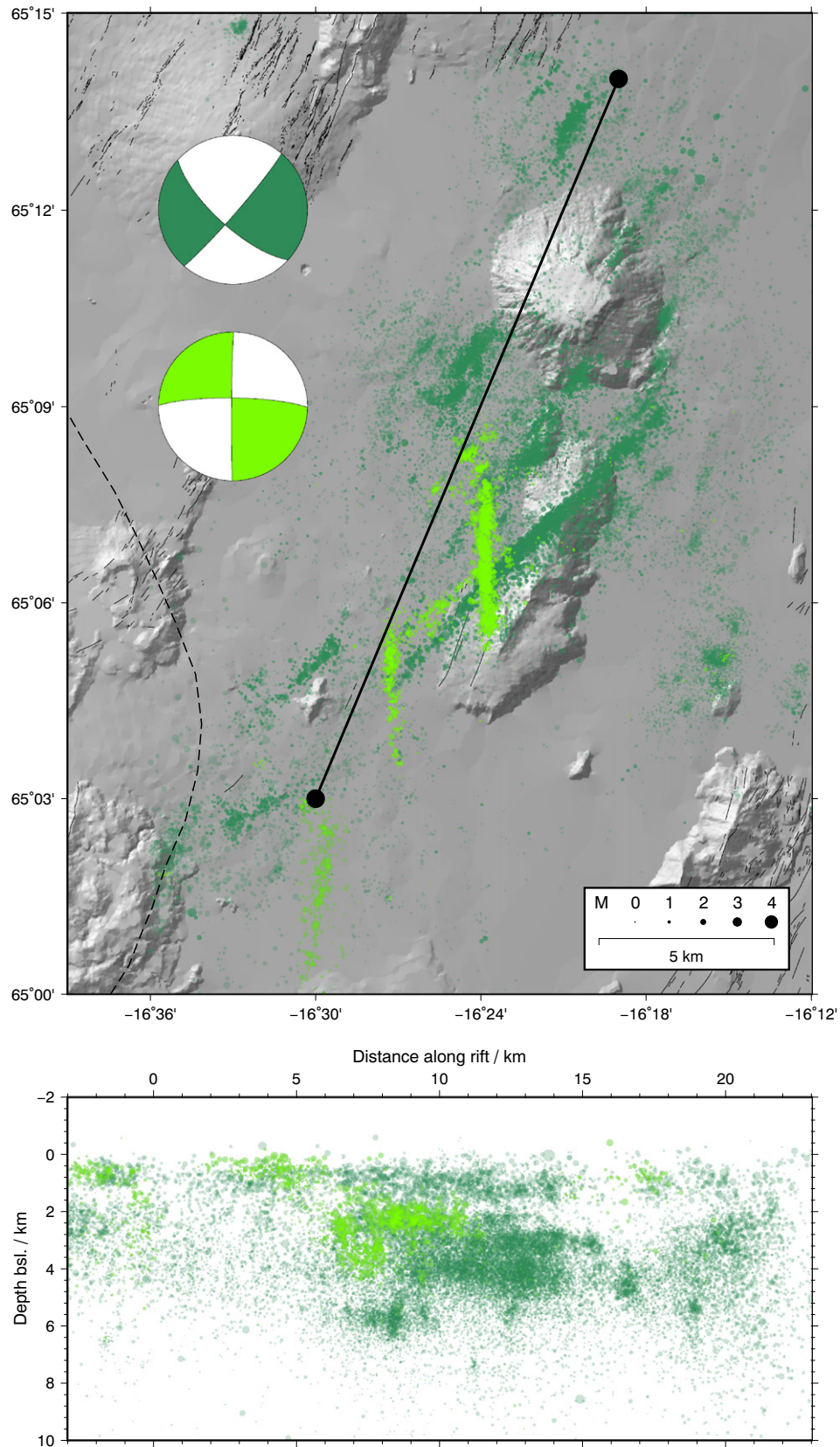


Fig. 5. Seismicity in the Askja-Herðubreið region. The detected and located seismicity is coloured green and scaled by the magnitude according to the scale in the lower-right panel. Dark green are earthquakes associated with northeast-southwest, left-lateral swarm; light green are earthquakes associated with north-south, right-lateral swarms. Representative fault plane solutions are shown for earthquakes in the north-south and northeast-southwest swarms. Lower panel shows the depth distribution of seismicity from south to north along the line indicated in the main panel.

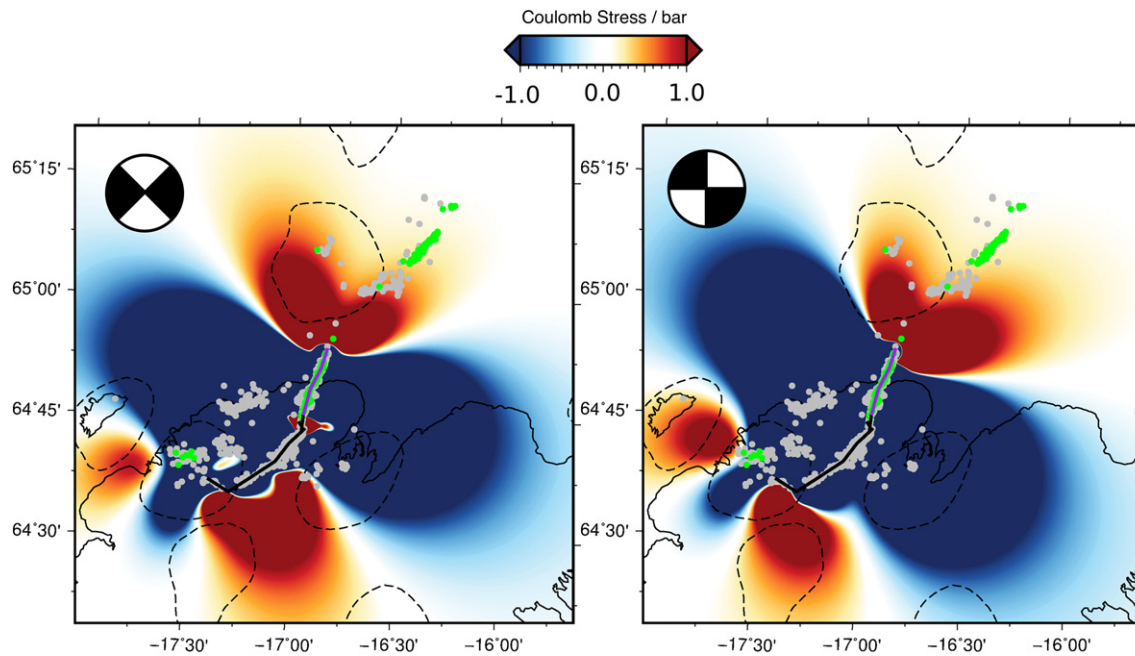


Fig. 6. Coulomb stresses calculated on NE-SW left-lateral faults (left panel) and N-S right-lateral faults (right panel) using COULOMB3 software (Lin and Stein Ross, 2004; Toda et al., 2011). The dyke opening model is from Green et al. (2015) and the dyke is delineated by the thick black line. Earthquake locations detected prior to 09/01/2014 are indicated by gray circles. Earthquakes detected on 09/01/2014 are indicated by the green circles. Central volcanoes and glaciers are delineated by dashed black lines and thin black lines respectively. The calculated coulomb stress is coloured using the scale bar on the right side and saturates at ± 1 bar.

snow during the winter and spring, followed by rapid melting during early summer. The same, asymmetric pattern is observed in the number of detected earthquakes in our catalogue (Fig. 8), suggesting that snow is also the cause of the seasonal variation in seismicity. We propose that the snow accumulation is driving changes in the seismicity rate by increasing the normal stress on the subsurface faults during the winter period relative to the summer period. Askja is a geothermal area, it is likely that there is a bigger range of fault and crack orientations than in those areas responding just to tectonically imposed stresses, where the faults are often tightly aligned (e.g., Green et al., 2014; Hjartardóttir et al., 2015). This would allow the change in vertical loading to affect a significant number of the active faults. The effect on the normal stress by the accumulation of snow can be calculated using $\sigma_v = \rho gh$, where ρ is the density of water (1000 kg m^{-3}), g is the gravitational strength in Iceland (9.823 ms^{-2}) and h is the equivalent depth of water. The calculated stress changes are on the order of 5 kPa (0.05 bar). This is similar to the stress changes as a result of tidal loading which have been observed to influence seismicity rates at mid-ocean ridges (Tolstoy et al., 2002), suggesting that the faults in this geothermal system are normally very close to failure.

Seasonal cycles in seismicity around other volcanoes have been observed around Kusatsu-Shirane Volcano in Japan (Nakano and Kumagai, 2005) and Ngauruhoe volcano in New Zealand (Jolly et al., 2012). In both cases the temporal variations are observed during restricted time periods and involve repeating long-period (LP) earthquakes. These earthquakes are located shallower than 1 km below the surface and are caused by the excitation of shallow gas filled cracks in shallow geothermal systems. The seasonality in both of these cases is due to the availability of meteoric water to the geothermal system. Around Askja, seasonal seismicity is not LP and is located significantly deeper (down to 3.5 km below surface). Any effect of larger amounts of water penetrating into the subsurface, possibly due to melting snow, would be more attenuated because of the larger depth. In addition, the lake Öskjuvatn must provide water to the geothermal reservoir and because it doesn't freeze in the winter there cannot be large changes in the pore fluid pressure which could change the seismicity rate.

3.2. Regional *b*-value analysis around Askja

The value of *b* from analysis of the magnitude-frequency distribution in regions around central Iceland are presented here. In order to produce statistically robust results each defined region must have >100 events within it. Around Askja the detected seismicity is split into three large regions: Herðubreið, Askja caldera and seismicity deeper than 10 km. Because of the large number of earthquakes around Askja, the large clusters can be subdivided further to analyze the temporal and spatial changes within each cluster.

3.2.1. Herðubreið

The region around the mountain Herðubreið has not been volcanically active since the last glacial maximum but is one of the most seismically active regions in Iceland. In this region, the overall *b*-value is 1.06 ± 0.02 , close to the global average. This suggests that the earthquakes occur in a relatively high stress region, especially compared to other regions in this area. However, there are large temporal changes in the *b*-value suggesting a more complex picture (Fig. 9).

Temporally, *b* varies between 1 and 2 over our observation period. During swarms (light blue bars, Fig. 9) *b* rapidly decreases to a value of approximately 1. More intense swarms (thicker blue bars, lower panel, Fig. 9) record a slow increase in *b* during the swarm. The rapid decrease in the observed value of *b* indicates that the region where the swarm earthquakes occur contains high stresses, which slowly decrease over the duration of the swarm, thus causing an increase in the *b*-value. In volcanic areas, earthquake swarms typically are caused by the intrusion of fluids into the crust. This causes the higher than usual *b*-values observed. The swarms we observe around Herðubreið are clearly induced by tectonic forces and do not involve interaction with fluids.

In tectonic regions, low *b*-values are associated with high stress asperities along major faults (i.e. Schorlemmer et al., 2004) and regions where large magnitude earthquakes nucleate (Wyss and Stefansson, 2006). After large tectonic earthquakes, *b* is observed to slowly increase after the mainshock, similar to the pattern observed around Herðubreið

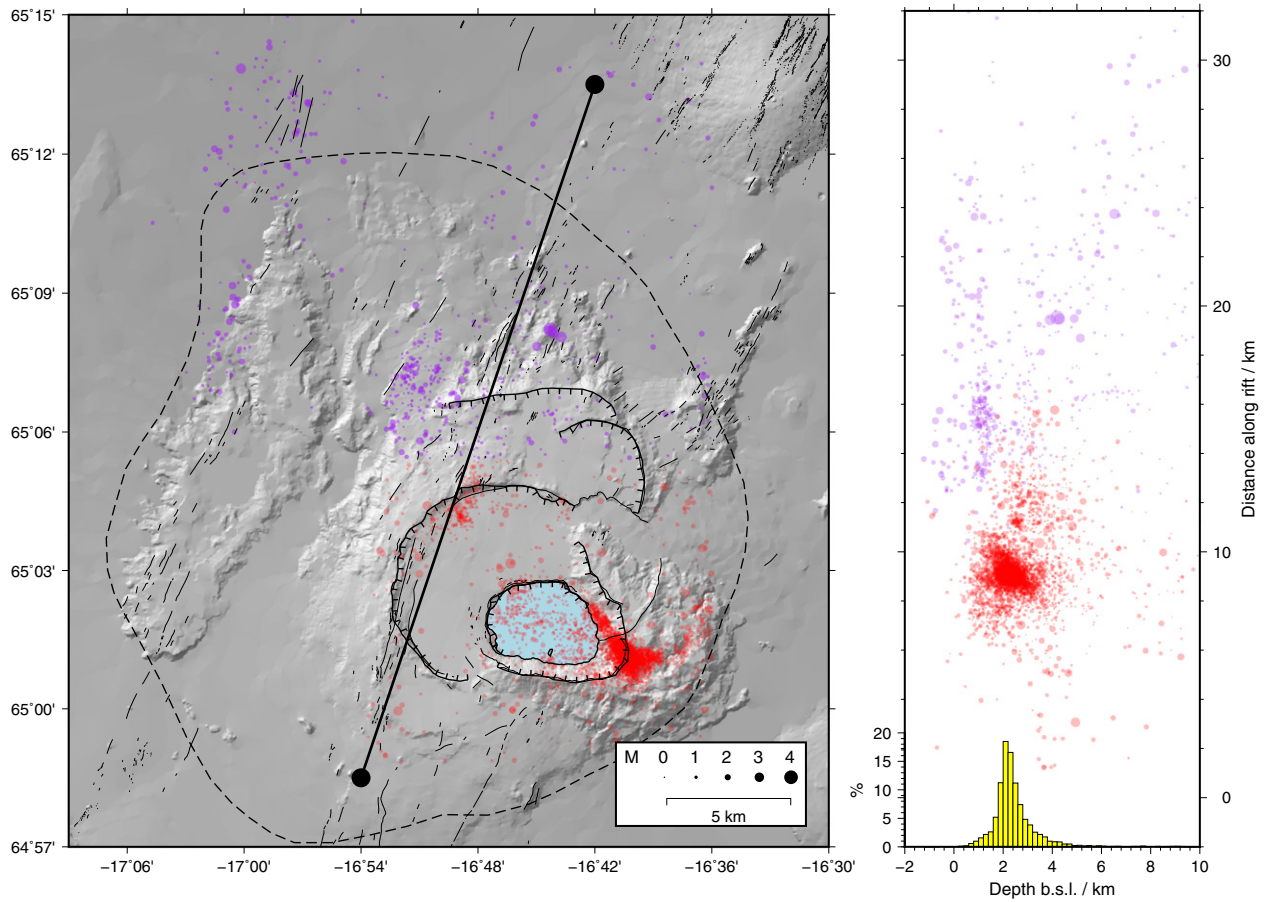


Fig. 7. Seismicity in the Askja caldera area. Seismicity in the Askja caldera catalogue is coloured red, while earthquakes in the West Askja catalogue are coloured purple. The earthquakes are scaled by their magnitude according to the scale in the lower-right panel. Right panel shows the depth distribution of seismicity from south to north along the line indicated in the main panel, with the histogram showing the depth distribution in the caldera. The lake Öskjuvatn is coloured light-blue.

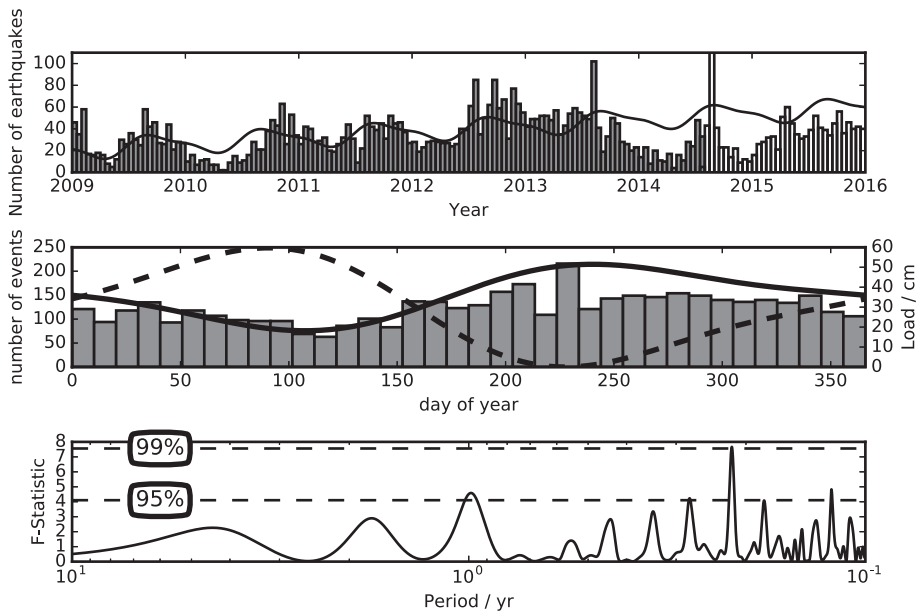


Fig. 8. The periodicity observed in earthquakes located around Askja’s caldera. Upper panel displays the number of earthquakes above magnitude 0.4 detected in ~15 day bins from 2009–December 2015. Overlain is the fit to the earthquake time series using Eq. (2). Middle panel shows the number of earthquakes detected in the same 10 day bins each year. A clear periodicity is observed with a minimum around day 100 and a maximum around day 220. Overlain is the fit to the earthquake time series using Eq. (2) (solid curve) and the calculated snow load from Drouin et al. (2017). The lower panel shows the F-statistic for periods calculated using a multi-taper Fourier transform. The 95% and 99% confidence values for 10 degrees of freedom are indicated by the horizontal, dashed lines.

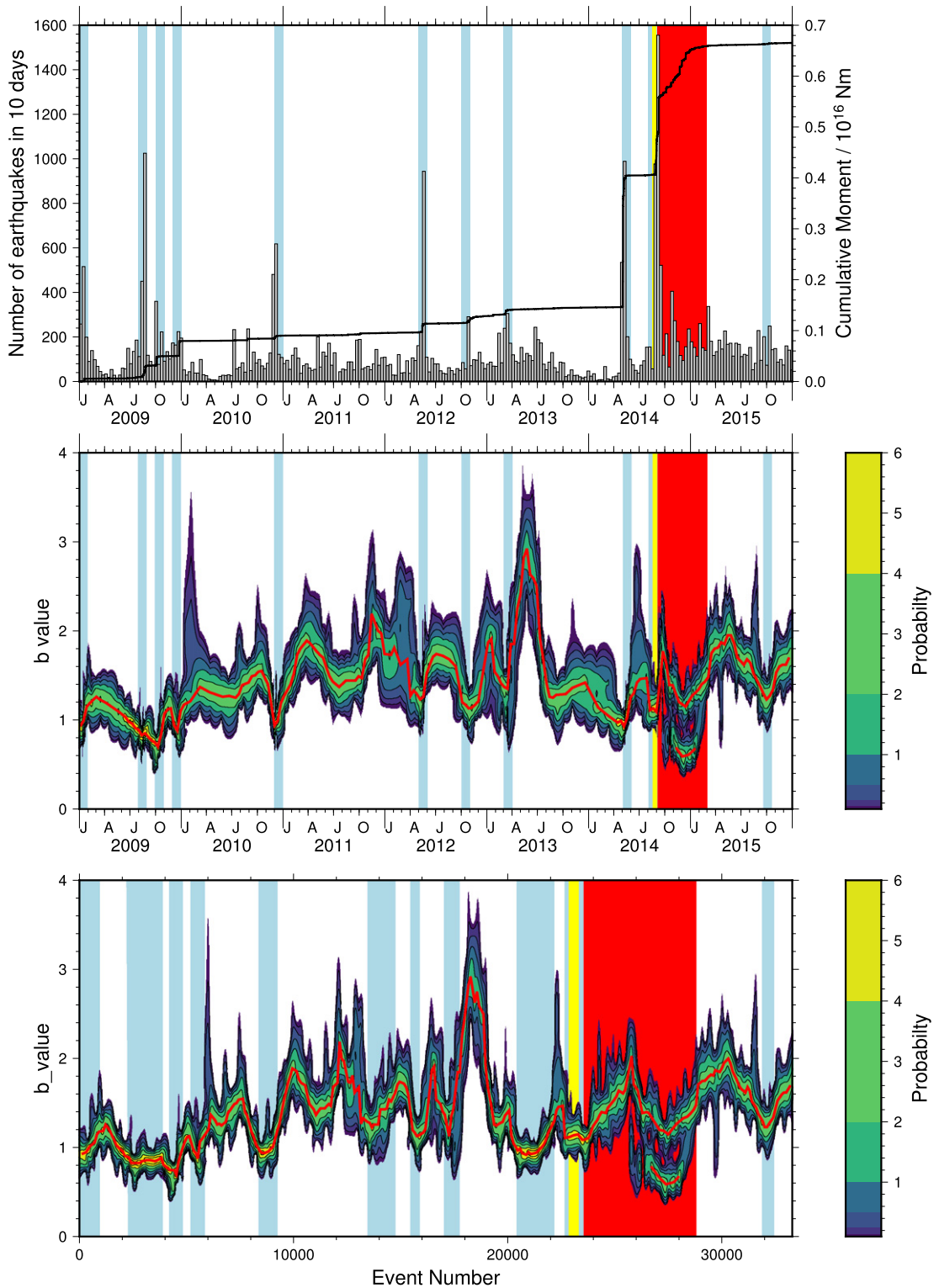


Fig. 9. Temporal variation in the b -value around Herðubreið. Upper panel indicates the number of earthquakes per day (gray boxes). Identified swarms are indicated by the light blue bands, while the dyke propagation period and subsequent eruption are indicated by the yellow and red bands respectively. Middle panel shows the probabilistic temporal variation in the b -value with time calculated using the method discussed in the text. The probability density is coloured by the indicated colour palette and the mode delineated by the red line. Lower panel is same as the middle panel but changes in seismicity rate are normalized by plotting the b -value temporal change by event number.

(Wiemer et al., 2002). The significantly larger size of the mainshock in most analyzed tectonic regions means that the time for b to return is much larger than we observe, reflecting the larger volume over which stresses must reduce.

Between swarms the value of b is variable but usually reaches a peak of approximately 2. These changes could be the result of large temporal changes in the stress of the region or it may be that the earthquakes between swarms sample different regions of the crust. We suggest that

such rapid changes in the stress of the region are unlikely and that the observed temporal changes reflect spatial heterogeneity of the stress.

3.2.2. Askja caldera

The seismicity around Askja caldera is dominated by the large number of earthquakes located to the east of the lake Öskjuvatn (see Figs. 1 and 7 for location). This is spatially associated with a large geothermal area where we may expect b to be >1 and highly variable (Trugman et al., 2016), due to the high temperatures and pore fluid pressures (Wyss, 1973; Wiemer and Wyss, 2002). Overall, the b -value around Askja is 1.21 ± 0.03 , significantly greater than the global average. Small, temporal changes in the b -value do occur (Fig. 10) but no large deviations are observed. At the start of our observation period the b -value is 0.95 and slowly increases to a value of 1.1 by the middle of 2011. Between mid-2011 and October 2012 the b -value increases to 1.6 and decreases back to a value of 1.1, peaking in April 2012. After this, the b -value recovers quickly to a value of 1.3 then stays approximately constant until February 2015. b then reduces to a value of 1 by the end of the observation period.

Temporal changes in the b -value around Askja suggest that there are long term changes in the geothermal system. These changes are unlikely to be related to the overall stress state as no large changes in the deformation are observed (de Zeeuw-van Dalfsen et al., 2013; Drouin et al., 2017). Instead, temporal changes are likely to be due to changes in the movement of fluids through the system. Such changes appear not to have affected the seismicity rate (Fig. 8) which does not change significantly over the duration of the study. The most significant b -value change is a large perturbation at the end of 2011. During the winter of 2011–2012 lake Öskjuvatn thawed significantly earlier than usual. This could be indicative of a short-term increase in the thermal or fluid flux through the geothermal system which could also cause higher than usual pore fluid pressures and accompanying higher b values.

Interestingly, the b -value in Askja caldera does not change during the Holuhraun dyke intrusion despite the stress changing in the area (Green et al., 2015) and seismicity levels briefly increasing (Fig. 8). From this observation, it follows that the increased number of earthquakes induced were located in the same fracture network as the 'usual' Askja seismicity and that the modest (1 bar) stress changes did not cause large changes in the fracture network. This observation has

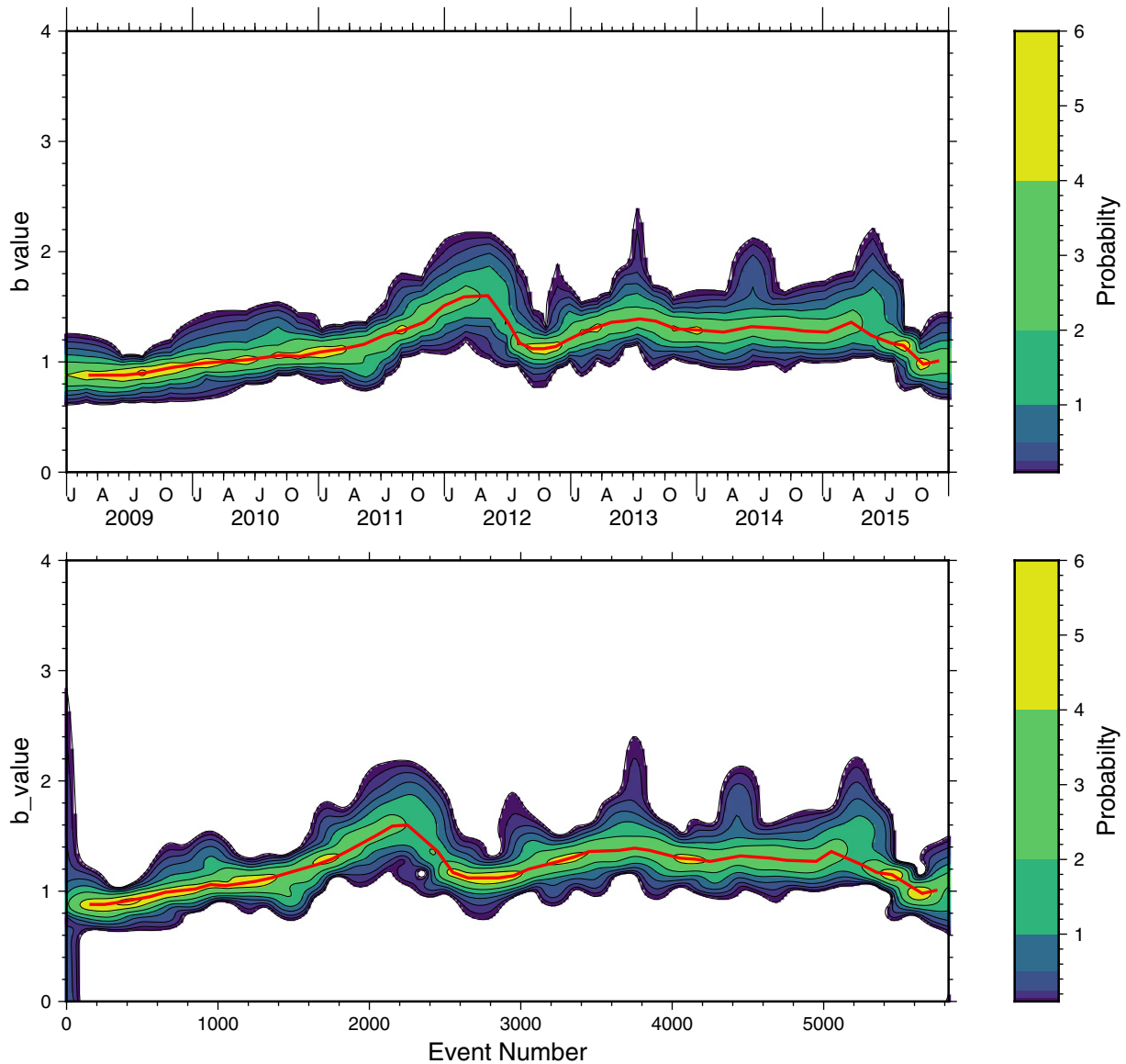


Fig. 10. Probabilistic temporal variation in the b -value around Askja. Upper panel shows the temporal variation in the b -value with time and the lower panel displays the temporal changes normalized by the seismicity rate. The probability density is coloured by the indicated colour palette and the mode delineated by the red line.

implications for stimulated geothermal reservoirs where low stress changes may not change the observed b -value. This will alter the chances of inducing a large earthquake and thus change the seismic hazard.

3.2.3. Deep seismicity

Overall the b -value of the seismicity deeper than 10 km bsl is 1.46 ± 0.06 with a M_c of 0.77. The large number of events in this region makes it possible to split it into six smaller sub-regions based on hypocentre location: four clusters are defined directly beneath Askja caldera, one beneath Kollóttadyngja shield volcano (see Fig. 1 for location) and one beneath Vaðalda shield volcano (see Fig. 1 for location). The b -values calculated for all clusters are summarized in Supplementary Table 3. Only one cluster (Askja 4) produced unstable b -values, as a result of the low number (76) of earthquakes in this cluster. Swarms of seismicity beneath Vaðalda were studied in detail by Greenfield and White (2015) who used cross-correlation based techniques to increase the number of detected earthquakes in 2012 by an order of magnitude compared to the original CMM catalogue. They calculated the b -value as 3.39 ± 0.17 .

All the deep clusters of earthquakes have b -values higher than 1, which, in volcanic regions suggests the presence of high temperatures and melt or other fluids (e.g., Wiemer and McNutt, 1997; Murru et al., 2007). The high b -value observations are consistent with the lower frequency content of these earthquakes and the imaged high V_p/V_s ratios (Greenfield et al., 2016) in the region around the earthquakes. All the evidence indicates that these earthquakes are induced by the movement of melt in persistently active regions of the crust.

3.3. b -values south of Askja during and after the 2014 dyke intrusion and subsequent eruption

The entire Bárðarbunga catalogue of >55,000 earthquakes has a b -value of 1.27 ± 0.02 . The temporal and spatial patterns in the b -value are analyzed by first splitting the earthquakes into a number of spatial clusters. Two spatial clusters are chosen (see Fig. 1 for locations): Bárðarbunga caldera and the path of the dyke intrusion. These two clusters of earthquakes are likely to be caused by different mechanisms. We discuss the b -values calculated for the caldera and dyke swarms.

3.3.1. Dyke b -values

The earthquakes along the dyke path have a high overall b -value of 1.43 ± 0.03 . This is clearly dominated by the huge number of earthquakes occurring during the propagation phase (69% of the total, Fig. 10) which has a similar b -value.

Fig. 10 shows the temporal changes in the b -value of the seismicity along the path of the dyke. A small reduction in the b -value occurs during the propagation period from ~ 3 at the start of the intrusion to ~ 2 at the end. When the main eruption starts on 31st August 2014, the b -value initially fluctuates between 1.5 and 6. By November 2014, the b -value stabilizes to ~ 4 and slowly decreases to a value of 3.2 till the end of the eruptive phase in February 2015. During the post-eruptive phase, b remains high for 4 months and then reduces to ~ 2 by October 2015 and stays constant till the end of the studied period. The large changes in b reflect many different processes occurring at the same time but can be used to infer the state of the dyke intrusion and how it changes through time.

In the first days of the dyke propagation (16–17 August 2014), detailed studies of the seismicity suggest that the dyke was traversing a

region above a deep, narrow melt feeder channel, which is therefore likely to be hot and may have contained some melt at the depth of the propagating dyke seismicity (Hudson et al., 2017). This caused the dyke to have few large earthquakes, but many small ones, with a 3 km-wide gap in seismicity along the initial dyke path; in this study, this is manifest as high b -values. Previous studies (Heimisson et al., 2015; Sigmundsson et al., 2015) have suggested that the path of the dyke is controlled by the lowest energy route when considering the gravitational potential energy due to topography and the strain energy due to plate spreading. Pauses between propagation periods (orange bars, Fig. 11) are thought to be due to the magmatic pressure having to increase in order to overcome energy barriers. This model might be expected to produce decreasing b -values between propagation phases due to increasing stress around the dyke and increasing b -values observed during propagation phases while the stress is being released. Alternatively, we might observe a similar pattern to around Herðubreifð (Section 3.2.1) where low b -values are observed during seismic swarms (propagation periods) as these are the regions with the highest stress.

In reality, neither of these models fits the observations particularly well. Some propagation periods have low b -values, some have high b -values, and some do not affect the b -value at all. This must reflect the spatial variability and complexity in the stresses and crustal properties as the dyke propagates forward. Some propagation periods do seem to match some of the expected observations. The longest stalling phase (20–23 August 2014) is before the dyke has to propagate through the highest energy barrier and thus the magma pressure must be high. We observe slowly decreasing b -values, indicating the slow build-up of stress around the dyke. Towards the end of the stalled period, the b -value fluctuates but a minimum in b is reached just before the next propagation phase. The b -value rapidly increases as the propagation phase starts again, possibly reflecting a rapid stress drop as the dyke passes the energy barrier. This model could apply for 9 of the 17 observed propagation phases where a decreasing b -value is observed in the stalled phase preceding the propagation phase.

Other magmatic intrusions are associated with high b -values, similar to those observed here (e.g., Wiemer et al., 1998) indicating that stresses required for dyke propagation are relatively low and/or that high pore fluid pressures are induced around the dyke. Studies analysing the temporal changes in b during multiple dyke intrusions in the same area are rare, but a sequence of dyke intrusions beneath El Hierro, Canary Islands (Roberts et al., 2016) is a good example. Each swarm, representing a dyke intrusion originating beneath the main edifice, was associated with a different b -value. The b -value varied between 1.0 and 3.5, similar to the range we observe for the Bárðarbunga-Holuhraun intrusion.

The variability in the b -value observations at both El Hierro and in Iceland indicate how important the pre-existing state of the crust is in producing the observed b -values. Perturbations in the b -value due to the additional stresses and fluids caused by the dyke intrusion modify this background b -value to produce the observed values. Frustratingly, because we do not usually observe earthquakes in regions where dykes are intruded it is difficult to assess the background b -value for the regions.

One clear signal in the b -value observations is the dramatic increase in the b -value after the start of the Holuhraun eruption in August 2014. This is well modelled as a large reduction in the stresses around the dyke caused by the system changing from a closed to an open system. Likewise, the end of the eruption in February 2015 is picked out by an increase in the seismicity rate and a small increase in the b -value

Fig. 11. Probabilistic temporal changes in the b -value in the Bárðarbunga – Holuhraun dyke. Upper panel shows the number of detected earthquakes per 10 days. Note the change of scale near the top of the plot. The lower 3 panels show the temporal variation in the b -value with time. The probability density is coloured by the indicated colour palette and the mode delineated by the red line. Orange stripes show periods of rapid dyke forward propagation, with stalled periods between them (from Ágústsdóttir et al., 2016). Panel b shows the complete time period from August 2014 to December 2015, Panel c shows a zoom around the dyke propagation period from 14th August–1st September 2014. Panel d shows the full catalogue where changes in seismicity rate are normalized by plotting the b -value temporal change by event number.

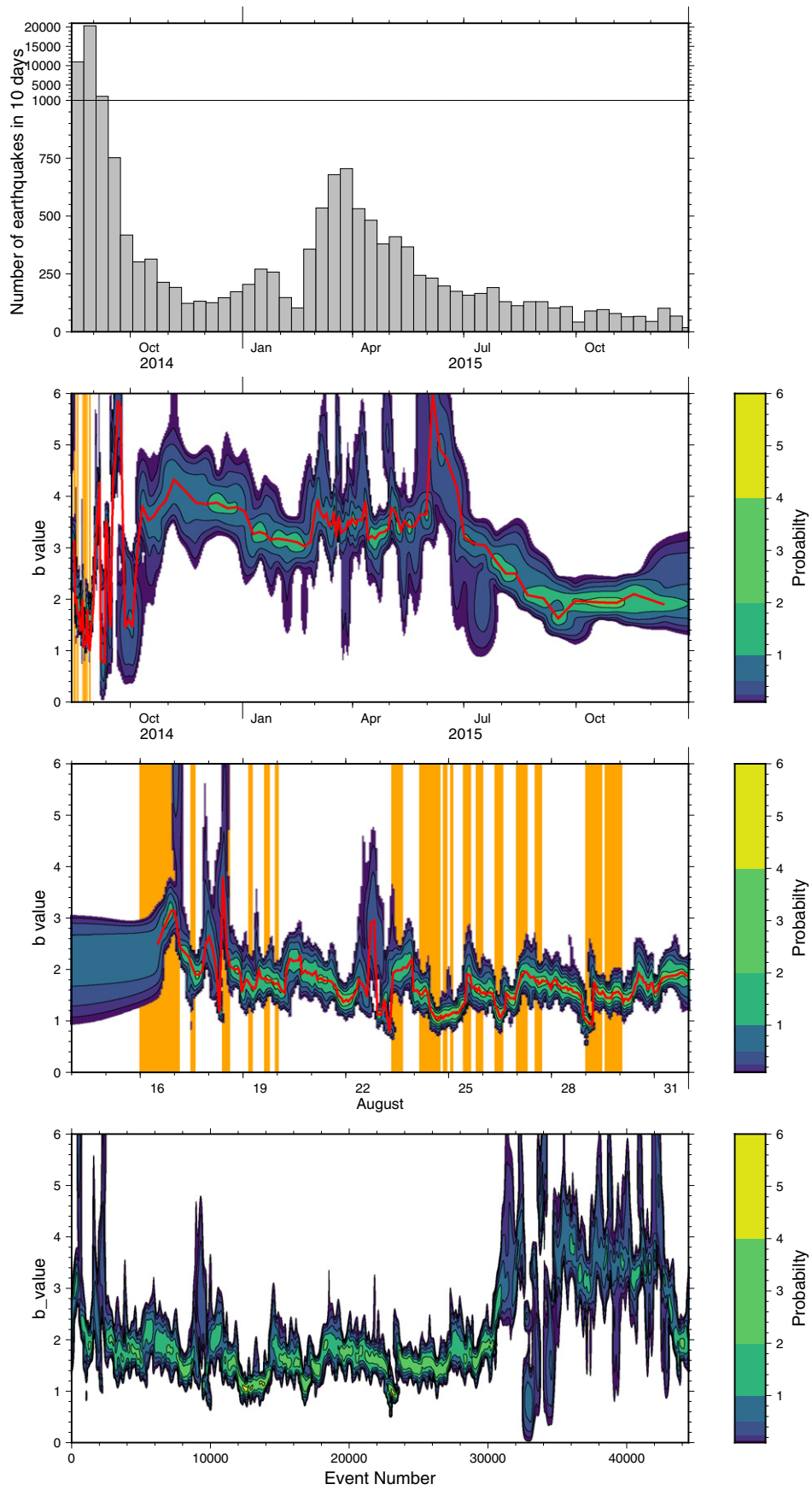


(Fig. 10). This is probably related to the low stresses induced during cooling of the dyke. The seismicity rate continues to decrease after this until it reaches a value of 2 (Fig. 10). This is likely to be caused by an increase in the stress, although, as the *b*-value is much higher than the global average of 1, the stresses must still be quite low. The decrease in *b* after the dyke intrusion is different to that observed at Mammoth Mountain, Long Valley Caldera, California (Wiemer et al., 1998) where the *b*-value remained high for at least 8 years following a magmatic intrusion.

3.3.2. Caldera *b*-values

The number of earthquakes located around Bárðarbunga caldera before the dyke intrusion and subsequent eruption in August 2014 is significantly smaller than that observed around Askja. As such, the temporal variations in the *b*-value before the dyke intrusion cannot be assessed. However, it is clear that before the dyke intrusion the *b*-value in Bárðarbunga caldera is 1.4. Background seismicity within the Bárðarbunga caldera is caused by the presence of an active geothermal system and tectonic faulting and elevated *b*-values are expected in such a region with high pore fluid pressures.

The initiation of dyke propagation in August 2014 causes the *b*-value to drop dramatically, reaching a minimum of 0.7 by September 2014. This coincides with the occurrence of a number of large ($M_w > 5.15$, indicated by the black pegs in Fig. 12) earthquakes. The reduction in *b*-value is likely to be caused by the sudden reduction in pressure in the magma storage region under Bárðarbunga and the onset of caldera collapse. This causes the applied stress to increase, thus reducing the *b*-value. As the overpressure in the magma chamber decreases, the magma discharge rate and the applied stresses decrease causing the *b*-value to slowly increase, reaching a value similar to the initial *b*-value by the time the subsidence stops (February 2015).

The recovery of the *b*-value back to background values indicates that the stress caused by the subsiding caldera has been completely relaxed and that there were no significant structural changes to the hydrothermal system. We might have expected such a large (65 m) amount of subsidence and numerous large magnitude earthquakes in the caldera to cause large changes in the fracture network exploited by the geothermal system. A lack of any large changes in the post-collapse *b*-value indicates that the geothermal system has remained stable. This may possibly be because the geothermal system already exploited fractures associated with similar earlier caldera collapses. Indeed, the eruptive craters formed during the most recent eruption at Holuhraun reused craters from the previous eruption which also initiated at Bárðarbunga.

3.4. *b*-values within geothermal areas across the Northern Volcanic Zone

Within the NVZ, three geothermal regions are sufficiently seismically active to reliably calculate and compare their *b*-values. We compare Askja (1.21 ± 0.03) and Bárðarbunga (1.2–1.3) with their high *b*-values to Krafla, in the north which has a significantly lower *b*-value (0.79 ± 0.04) (Schuler et al., 2016). The main difference between the three sites is that Askja and Bárðarbunga are natural geothermal sites while Krafla is actively exploited for both power and heating.

The *b*-values within the Askja and Bárðarbunga geothermal areas are higher than the global average of 1 and similar to those observed in other natural un-exploited geothermal reservoirs around the world (e.g., Farrell et al., 2009; Trugman et al., 2016; Wilks et al., 2017). The high *b*-values are caused by the high pore fluid pressures, which reduce the effective stress across fractures.

In contrast, the low *b*-values around Krafla must reflect differences in the local stresses and fracture network. We can discount any differences due to the Krafla rifting episode between 1975 and 1984. Firstly, because *b*-values in the Bárðarbunga caldera had returned to background values by the time the eruption had ended and *b*-values in the

Askja caldera were unchanged despite significant stress changes due to the dyke intrusion. Secondly, *b*-values calculated by Arnott and Foulger (1994) for seismicity around Krafla in the summer of 1985, just after the end of the rifting episode, are comparable to those of Schuler et al. (2016), indicating that the *b*-value has not changed significantly since the end of the 1974–1985 Krafla rifting episode.

It appears that the power station has a negligible impact on the *b*-value. Other geothermal areas which are actively exploited also typically exhibit high *b*-values (e.g., the Geysers field, Kamer and Hiemer, 2015; Trugman et al., 2016) making Krafla an exception. Temporal changes in the *b*-value in the Geysers field do occur, particularly during changes in injection rate, but usually increase the *b*-value before recovering back to their background value (Bachmann et al., 2012; Shapiro et al., 2013). Re-injection of water does occur in Krafla, but doesn't increase the *b*-values to those seen at other geothermal areas. Additionally, the lack of significant change of the *b*-value between 1985 and 2015, despite extraction of steam over the entire period suggests that the power plant has a negligible impact on *b* around Krafla and the *b*-value we observe is the background *b*-value.

While a definite cause cannot be placed on the low *b*-values observed at Krafla, it is clear that the system behaves differently to Askja and Bárðarbunga.

4. Conclusions

The seismicity around Askja from 2009 to 2015 and around Bárðarbunga from 2013 to 2015 has been detected and located. Local magnitudes are calculated for all ~100,000 earthquakes using a newly developed local magnitude scale appropriate for use in central Iceland.

The seismicity around Askja is clustered into four distinct regions: 1) west of Askja, 2) Askja caldera, 3) close to Mt. Herðubreið and 4) deeper than 10 km bsl. Cluster 1, to the west of Askja is the least active region and during the studied period was only active in 2009 and 2011. The low *b*-values and normal faulting fault plane solutions reveal this to be a region accommodating a small portion of the extensional strain. In cluster 2, within the Askja caldera, earthquakes are mostly found beneath the active geothermal region associated with the most recently formed caldera, Öskjuvatn. *b*-Values only vary slightly with time in this region, but strong seasonal variations in the number of earthquakes detected are recorded. The number of earthquakes is at a minimum during the spring when the snow depth is at a maximum. We show that vertical stress changes on the order 5 kPa modulate the frequency of earthquakes. In contrast, in cluster 3 around Herðubreið, temporal changes in the *b*-value are clear. *b* is low during earthquake swarms but higher during inter-swarm periods, indicating that different mechanisms are inducing seismicity during swarm periods. Newly identified north-south orientated right-lateral strike-slip faults around Herðubreið suggest that extension in this area is accommodated by conjugate fault pairs, with the entire region becoming more active as a result of the increase in Coulomb stress caused by the 2014 dyke intrusion to the south. Cluster 4, the earthquakes in the deep – usually ductile – portion of the crust have high *b*-values, confirming previous interpretations that these earthquakes are caused by the movement of melt in the mid-crust.

Analyses of the temporal and spatial changes in the *b*-value of earthquakes induced by the Bárðarbunga-Holuhraun dyke intrusion show that the *b*-value is high along the dyke path during the first day, where the dyke propagated through crust above a small vertical seismically inferred melt feeder channel: this region is therefore likely to be hotter than along the rest of the dyke path. After the first day, the *b*-value then reduced slightly but remained above 1 until the dyke propagation ended 13 days later. At Bárðarbunga caldera, *b*-values reduced significantly when the dyke started propagating but returned to background values when the eruption ended,

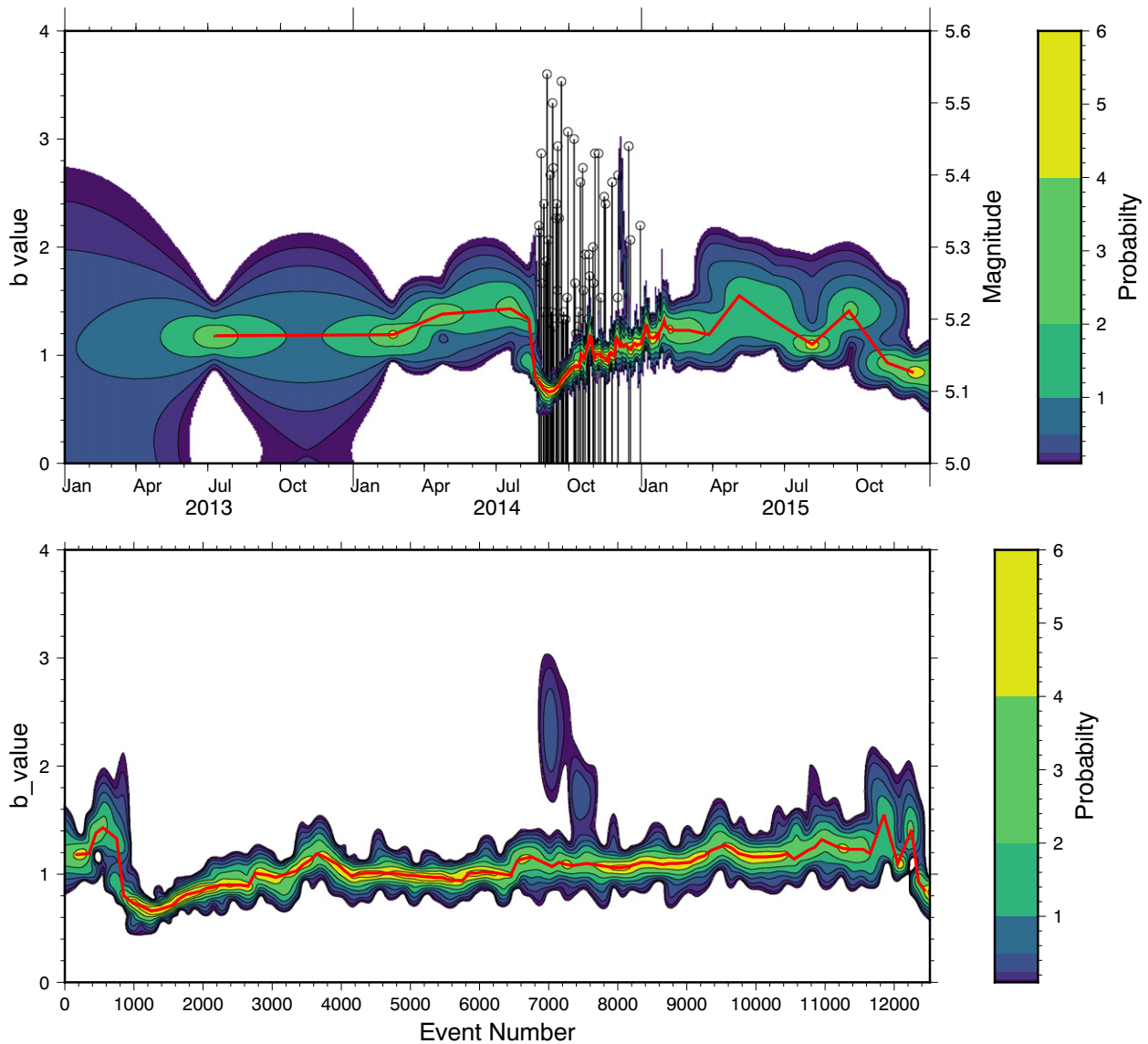


Fig. 12. Temporal changes in the b-value for earthquakes within the Bárðarbunga caldera. Upper panel shows the temporal variation in the b-value with time. The b-value probability density is coloured by the indicated colour palette and the mode delineated by the red line. Earthquakes larger than Mw 5.15 as recorded by the IMO catalogue are indicated by the black lines. Lower panel is same as the upper panel but changes in seismicity rate are normalized by plotting the b-value temporal change by event number.

most likely due to the removal of the driving stress from the underlying subsiding caldera.

Supplementary data to this article can be found online at <https://doi.org/10.1016/j.jvolgeores.2018.08.010>.

Acknowledgements

Seismometers were borrowed from the Natural Environmental Research Council (NERC) SEIS-UK facility (loans 857, 914, 968, 980 and 1022) and the work funded by research grants from the NERC (NE/F011407, NE/H025006, NE/L013932/1 and NE/M017427) and by a PhD studentship for TG funded by Shell UK. We also acknowledge funding from the European Community's Seventh Framework Programme grant 308377 (Project FUTUREVOLC). We thank all those who participated in downloading the data from the field over the years. In particular, we thank Bryndís Brandsdóttir and Sveinbjörn Steinþórsson, without whom this project would not have been possible. Chris Bean (University College Dublin), the British Geological Survey and the Icelandic

Meteorological Office (IMO) kindly provided additional data from their seismometers in north-east Iceland. Useful comments by three anonymous reviewers and the editor Philippe Jousset improved the quality of this manuscript. Some figures were generated using Generic Mapping Tools (Wessel et al., 2013), and ObsPy (Beyreuther et al., 2010) was used extensively to analyze the data. Dept. Earth Sciences, Cambridge publication number ESC4316.

References

- Ader, T.J., Avouac, J.-P., 2013. Detecting periodicities and declustering in earthquake catalogues using the Schuster spectrum, application to Himalayan seismicity. *Earth Planet. Sci. Lett.* 377–378, 97–105. <https://doi.org/10.1016/j.epsl.2013.06.032>.
- Ágústsdóttir, T., Woods, J., Greenfield, T., Green, R.G., White, R.S., Winder, T., et al., 2016. Strike-slip faulting during the 2014 Bárðarbunga-Holuhraun dyke intrusion, central Iceland. *Geophys. Res. Lett.* 43, 1495–1503.
- Aki, K., 1965. Maximum likelihood estimate of b in the formula $\log N = a - bM$ and its confidence limits. *Bull. Earthq. Res. Inst., Univ. Tokyo* 237–239.
- Árnadóttir, T., Lund, B., Jiang, W., Geirsson, H., Björnsson, H., Einarsson, P., Sigurdsson, T., 2009. Glacial rebound and plate spreading: results from the first countrywide GPS observations in Iceland. *Geophys. J. Int.* 177, 691–716.

- Arnott, S.K., Foulger, G.R., 1994. The Krafla spreading segment, Iceland 1. Three-dimensional crustal structure and the spatial and temporal distribution of local earthquakes. *J. Geophys. Res.* 99, 23801–23825.
- Bachmann, C.E., Wiemer, S., Goertz-Allmann, B.P., Woessner, J., 2012. Influence of pore-pressure on the event-size distribution of induced earthquakes. *Geophys. Res. Lett.* 39 (9) (n/a–n/a).
- Beyreuther, M., Barsch, R., Krischer, L., Megies, T., Behr, Y., Wassermann, J., 2010. ObsPy: a Python toolbox for seismology. *Seismol. Res. Lett.* 81, 530–533.
- Cao, A.M., Gao, S.S., 2002. Temporal variation of seismic b-values beneath northeastern Japan island arc. *Geophys. Res. Lett.* 29 (9) (<Go to ISI://WOS:000178888000029).
- Carey, R.J., Houghton, B.F., Thordarson, T., 2010. Tephra dispersal and eruption dynamics of wet and dry phases of the 1875 eruption of Askja Volcano, Iceland. *Bull. Volcanol.* 72, 259–278.
- DeMets, C., Gordon, R.G., Argus, D.F., 2010. Geologically current plate motions. *Geophys. J. Int.* 181, 1–80.
- Drew, J., White, R.S., Tilmann, F., Tarasewicz, J., 2013. Coalescence microseismic mapping. *Geophys. J. Int.* 195, 1773–1785.
- Drouin, V., Sigmundsson, F., Ófeigsson, B.G., Hreinsdóttir, S., Sturkell, E., Einarsson, P., 2017. Deformation in the Northern Volcanic Zone of Iceland 2008–2014: an interplay of tectonic, magmatic, and glacial isostatic deformation. *J. Geophys. Res. Solid Earth* 122 (4), 3158–3178.
- Einarsson, P., Brandsdóttir, B., Gudmundsson, M.T., Björnsson, H., Gronvold, K., Sigmundsson, F., 1997. Center of the Iceland hotspot experiences volcanic unrest. *Eos* 78 (35), 374–375.
- El-Isa, Z.H., Eaton, D.W., 2014. Spatiotemporal variations in the b-value of earthquake magnitude–frequency distributions: classification and causes. *Tectonophysics* 615, 1–11 (<Go to ISI://WOS:000333003000001).
- Farrell, J., Husen, S., Smith, R.B., 2009. Earthquake swarm and b-value characterization of the Yellowstone volcano-tectonic system. *J. Volcanol. Geotherm. Res.* 188, 260–276.
- Green, R.G., White, R.S., Greenfield, T., 2014. Motion in the north Iceland volcanic rift zone accommodated by bookshelf faulting. *Nat. Geosci.* 7, 29–33.
- Green, R.G., Greenfield, T., White, R.S., 2015. Triggered earthquakes suppressed by an evolving stress shadow from a propagating dyke. *Nat. Geosci.* 8, 629–632.
- Greenfield, T., White, R.S., 2015. Building Icelandic igneous crust by repeated melt injections. *J. Geophys. Res.* 120, 1–14.
- Greenfield, T., White, R.S., Roecker, S., 2016. The magmatic plumbing system of the Askja central volcano, Iceland, as imaged by seismic tomography. *J. Geophys. Res. Solid Earth* 121.
- Gudmundsson, M.T., Jónsdóttir, K., Hooper, A., Holohan, E.P., Halldórsson, S.A., Ófeigsson, B.G., et al., 2016. Gradual caldera collapse at Bárðarbunga volcano, Iceland, regulated by lateral magma outflow. *Science* 353.
- Heimisson, E.R., Hooper, A., Sigmundsson, F., 2015. Forecasting the path of a laterally propagating dyke. *J. Geophys. Res.* 120.
- Hjartardóttir, R.S., Einarsson, P., Magnúsdóttir, S., Björnsdóttir, P., Brandsdóttir, B., 2015. Fracture systems of the Northern Volcanic Rift Zone, Iceland: an onshore part of the Mid-Atlantic plate boundary. *Geol. Soc. Lond., Spec. Publ.* 420, 297–314.
- Hudson, T.S., White, R.S., Greenfield, T., Ágústsdóttir, T., Brisbourne, A., Green, R.G., 2017. Deep crustal melt plumbing of Bárðarbunga volcano, Iceland. *Geophys. Res. Lett.* 44 (17), 8785–8794. <https://doi.org/10.1002/2017GL074749>.
- Hutton, L.K., Boore, D.M., 1987. The Ml Scale in Southern-California. *Bull. Seismol. Soc. Am.* 77 (6), 2074–2094 (<Go to ISI://WOS:A1987K990500011).
- Illsley-Kemp, F., Keir, D., Bull, J.M., Ayele, A., Hammond, J.O.S., Kendall, J.M., et al., 2017. Local Earthquake Magnitude Scale and b-Value for the Danakil Region of Northern Afar. *Bull. Seismol. Soc. Am.* 107 (2), 521–531. <http://www.bssaonline.org/content/107/2/521.abstract>.
- Jolly, A.D., Neuberger, J., Jousset, P., Sherburn, S., 2012. A new source process for evolving repetitive earthquakes at Ngauruhoe volcano, New Zealand. *J. Volcanol. Geotherm. Res.* 215–216, 26–39.
- Kamer, Y., Hiemer, S., 2015. Data-driven spatial b value estimation with applications to California seismicity: to b or not to b. *J. Geophys. Res.* 120, 5191–5214.
- Karson, J.A., 2017. The Iceland Plate Boundary Zone: propagating rifts, migrating transforms, and rift-parallel strike-slip faults. *Geochem. Geophys. Geosyst.* 18 (11), 4043–4054.
- Keir, D., Stuart, G.W., Jackson, A., Ayele, A., 2006. Local earthquake magnitude scale and seismicity rate for the Ethiopian rift. *Bull. Seismol. Soc. Am.* 96, 2221–2230.
- Key, J., White, R.S., Soosalu, H., Jakobsdóttir, S.S., 2011a. Correction to “Multiple melt injection along a spreading segment at Askja, Iceland”. *Geophys. Res. Lett.* 38, 900041.
- Key, J., White, R.S., Soosalu, H., Jakobsdóttir, S.S., 2011b. Multiple melt injection along a spreading segment at Askja, Iceland. *Geophys. Res. Lett.* 38.
- Larsen, G., Gudmundsson, M.T., 2015. In: Ilyinskaya, E., Larsen, G., Gudmundsson, M.T. (Eds.), *The Bardarbunga Volcanic System*.
- Latham, G.V., Warren, N.W., 1970. An experimental study of thermally induced microfracturing and its relation to volcanic seismicity. *J. Geophys. Res.* 75, 4455–4464.
- Lin, J., Stein Ross, S., 2004. Stress triggering in thrust and subduction earthquakes and stress interaction between the southern San Andreas and nearby thrust and strike-slip faults. *J. Geophys. Res. Solid Earth* 109 (B2). <https://doi.org/10.1029/2003JB002607>.
- Lomax, A., Virieux, J., Volant, P., Berge, C., 2000. Probabilistic earthquake location in 3D and layered models: introduction of a Metropolis-Gibbs method and comparison with linear locations. In: Thurber, C.H., Rabinowitz, N. (Eds.), *Advances in Seismic Event Location*. Kluwer, Amsterdam, pp. 101–134.
- Murru, M., Console, R., Falcone, G., Montuori, C., SgROI, T., 2007. Spatial mapping of the b value at Mount Etna, Italy, using earthquake data recorded from 1999 to 2005. *J. Geophys. Res. Solid Earth* 112, 1–15.
- Nakano, M., Kumagai, H., 2005. Response of a hydrothermal system to magmatic heat inferred from temporal variations in the complex frequencies of long-period events at Kusatsu-Shirane Volcano, Japan. *J. Volcanol. Geotherm. Res.* 147 (3–4), 233–244.
- Pedersen, R., Sigmundsson, F., Masterlark, T., 2009. Rheologic controls on inter-rifting deformation of the Northern Volcanic Zone, Iceland. *Earth Planet. Sci. Lett.* 281, 14–26.
- Prieto, G.A., Parker, R.L., Vernon III, F.L., 2009. A Fortran 90 library for multitaper spectrum analysis. *Comput. Geosci.* 35 (8), 1701–1710. <http://dl.acm.org/citation.cfm?id=1576862.1577037>.
- Richter, C.F., 1935. An instrumental earthquake magnitude scale. *Bull. Seismol. Soc. Am.* 25, 1–32.
- Roberts, N.S., Bell, A.F., Main, I.G., 2015. Are volcanic seismic b-values high, and if so when? *J. Volcanol. Geotherm. Res.* 308, 127–141.
- Roberts, N.S., Bell, A.F., Main, I.G., 2016. Mode switching in volcanic seismicity: El Hierro 2011–2013. *Geophys. Res. Lett.* 43 (9), 4288–4296.
- Scholz, C.H., 1968. Microfracturing and the inelastic deformation of rock in compression. *J. Geophys. Res.* 73, 1417.
- Schorlemmer, D., Wiemer, S., Wyss, M., 2004. Earthquake statistics at Parkfield: 1. Stationary of values. *J. Geophys. Res.* 109 (B12).
- Schuler, J., Pugh, D.J., Hauksson, E., White, R.S., Stock, J.M., Brandsdóttir, B., 2016. Focal mechanisms and size distribution of earthquakes beneath the Krafla central volcano, NE Iceland. *J. Geophys. Res. Solid Earth* 121, 1–17.
- Schuster, A., 1897. On lunar and solar periodicities of earthquakes. *Proc. R. Soc. Lond.* 61, 455–465.
- Shapiro, S.A., Krüger, O.S., Dinske, C., 2013. Probability of inducing given-magnitude earthquakes by perturbing finite volumes of rocks. *J. Geophys. Res. Solid Earth* 118 (7), 3557–3575.
- Shi, Y., Bolt, B., 1982. The standard error of the magnitude-frequency b value. *Bull. Seismol. Soc. Am.* 72, 1677–1687.
- Sigmundsson, O., Halldórsson, S., 2015. Delimiting Bárðarbunga and Askja volcanic systems with Sr- and Nd-isotope ratios. *Jökull* 65.
- Sigmundsson, O., Karlsson, H.R., Larsen, G., 2000. The 1996 and 1998 subglacial eruptions beneath the Vatnajökull ice sheet in Iceland: contrasting geochemical and geophysical inferences on magma migration. *Bull. Volcanol.* 61 (7), 468–476. <https://doi.org/10.1007/PL00008912>.
- Sigmundsson, F., Hooper, A., Hreinsdóttir, S., Vogfjörð, K.S., Ófeigsson, B.G., Heimisson, E.R., et al., 2015. Segmented lateral dyke growth in a rifting event at Bárðarbunga volcanic system, Iceland. *Nature* 517, 191–195.
- Soosalu, H., Key, J., White, R.S., Knox, C., Einarsson, P., Jakobsdóttir, S.S., 2010. Lower-crustal earthquakes caused by magma movement beneath Askja volcano on the North Iceland rift. *Bull. Volcanol.* 72, 55–62.
- Sturkell, E., Sigmundsson, F., Slunga, R., 2006. 1983–2003 decaying rate of deflation at Askja caldera: pressure decrease in an extensive magma plumbing system at a spreading plate boundary. *Bull. Volcanol.* 68, 727–735.
- Thorarinnsson, S., 1962. The Eruption in Askja, 1961 a preliminary report. *Am. J. Sci.* 260, 641–651.
- Toda, S., Stein, R.S., Sevilgen, V., Lin, J., 2011. Coulomb 3.3 Graphic-rich deformation and stress-change software for earthquake, tectonic, and volcano research and teaching—user guide. *U.S. Geological Survey Open-File Report* 2011–1060.
- Tolstoy, M., Vernon, F.L., Orcutt, J.A., Wyatt, F.K., 2002. Breathing of the seafloor: tidal correlations of seismicity at Axial volcano. *Geology* 30 (6), 503–506. [https://doi.org/10.1130/0091-7613\(2002\)030](https://doi.org/10.1130/0091-7613(2002)030).
- Trugman, D.T., Shearer, P.M., Borsa, A.A., Fialko, Y., 2016. A comparison of long-term changes in seismicity at the Geysers, Salton Sea, and Coso geothermal fields. *J. Geophys. Res. Solid Earth* 121 (1), 225–247.
- Urhammer, R.A., 1982. The optimal estimation of earthquake parameters. *Phys. Earth Planet. Inter.* 4, 1369–1379.
- Wessel, P., Smith, W.H.F., Scharroo, R., Luis, J., Wobbe, F., 2013. Generic mapping tools: improved version released. *EOS Trans. Am. Geophys. Union* 94, 409–410.
- Wiemer, S., McNutt, S.R., 1997. Variations in the frequency–magnitude distribution with depth in two volcanic areas: Mount St. Helens, Washington, and Mt. Spurr, Alaska. *Geophys. Res. Lett.* 24 (2), 189–192.
- Wiemer, S., Wyss, M., 2002. Mapping spatial variability of the frequency–magnitude distribution of earthquakes. *Adv. Geophys.* 45, 259–302.
- Wiemer, S., McNutt, S.R., Wyss, M., 1998. Temporal and three-dimensional spatial analyses of the frequency–magnitude distribution near Long Valley Caldera, California. *Geophys. J. Int.* 134, 409–421.
- Wiemer, S., Gerstenberger, M., Hauksson, E., 2002. Properties of the aftershock sequence of the 1999 Mw 7.1 Hector Mine earthquake: implications for aftershock hazard. *Bull. Seismol. Soc. Am.* 92 (4), 1227–1240.
- Wilks, M., Kendall, J.M., Nowacki, A., Biggs, J., Wookey, J., Birhanu, Y., et al., 2017. Seismicity associated with magmatism, faulting and hydrothermal circulation at Aluto Volcano, Main Ethiopian Rift. *J. Volcanol. Geotherm. Res.* 340, 52–67.
- Woods, J., Donaldson, C., White, R.S., Brandsdóttir, B., Caudron, C., Hudson, T.S., Ágústsdóttir, T., 2018. Long-period seismicity reveals magma pathways above a propagating dyke during the 2014–15 Bárðarbunga rifting episode, Iceland. *Earth Planet. Sci. Lett.* 490, 216–219. <https://doi.org/10.1016/j.epsl.2018.03.020>.
- Wyss, M., 1973. Towards a physical understanding of the earthquake frequency distribution. *Geophys. J. Int.* 31, 341–359.
- Wyss, M., Stefansson, R., 2006. Nucleation points of recent mainshocks in southern Iceland, mapped by b-values. *Bull. Seismol. Soc. Am.* 96, 599–608.
- de Zeeuw-Van Dalssen, E., Rymer, H., Sigmundsson, F., Sturkell, E., 2005. Net gravity decrease at Askja volcano, Iceland: constraints on processes responsible for continuous caldera deflation, 1988–2003. *J. Volcanol. Geotherm. Res.* 139, 227–239.
- de Zeeuw-van Dalssen, E., Rymer, H., Sturkell, E., Pedersen, R., Hooper, A., Sigmundsson, F., Ófeigsson, B.G., 2013. Geodetic data shed light on ongoing caldera subsidence at Askja, Iceland. *Bull. Volcanol.* 75, 709.